THE ASTROPHYSICAL JOURNAL, 473:L37–L40, 1996 December 10

THE GEMINGA PULSAR: SOFT X-RAY VARIABILITY AND AN *EUVE* OBSERVATION

JULES P. HALPERN
Columbia Astrophysics Laboratory, Columbia University, 538 West 120th Street, New York, NY 10027; jules@carmen.phys.columbia.edu
CHRISTOPHER MARTIN
Downs Laboratory, California Institute of Technology, 220-47, Pasadena, CA 91125; cmartin@porgy.srl.caltech.edu
AND
HERMAN L. MARSHALL
Center for Space Research, Massachusetts Institute of Technology, 37-667a, Cambridge, MA 02139; hermanm@space.mit.edu
Received 1996 July 16; accepted 1996 September 26

ABSTRACT

We observed the Geminga pulsar with the *EUVE* satellite, detecting pulsed emission in the Deep Survey imager. Joint spectral fits of the *EUVE* flux with *ROSAT* PSPC data are consistent with thermal plus power-law models in which the thermal component makes the dominant contribution to the soft X-ray flux seen by *EUVE* and *ROSAT*. The data are consistent with blackbody emission of $T = (4-6) \times 10^5$ K over most of the surface of the star at the measured parallax distance of 160 pc. Although model atmospheres are more realistic, and can fit the data with effective temperatures a factor of 2 lower, current data would not discriminate between these and blackbody models. We also find evidence for variability of Geminga's soft X-ray pulse shape. Narrow dips in the light curve that were present in 1991 had largely disappeared in 1993/1994, causing the pulsed fraction to decline from 32% to 18%. If the dips are attributed to cyclotron resonance scattering by an $e^{\pm}$ plasma on closed magnetic field lines, then the process that resupplies that plasma must be variable.

Subject headings: pulsars: individual (Geminga) — stars: neutron — X-rays: stars

1. INTRODUCTION

The high-energy γ-ray source Geminga is the only known radio-quiet rotation-powered pulsar, with $P = 0.237$ s and characteristic age $P/2\dot{P} = 3.4 \times 10^5$ yr (Halpern & Holt 1992; Bertsch et al. 1992). A parallax distance of 160 pc has been measured with the *Hubble Space Telescope* (*HST*) (Caraveo et al. 1996). A soft X-ray study of Geminga with the *ROSAT* Position Sensitive Proportional Counter (PSPC) revealed two components, distinct in both their spectra and light curves (Halpern & Ruderman 1993). While the dominant, softer component was demonstrably thermal emission from the surface of the neutron star, a harder tail was present that could equally well be described as either a nonthermal power law or a hotter blackbody. Recent *ASCA* observations resolved the nature of the hard component in favor of nonthermal emission (Halpern & Wang 1996). Thus, there is no longer evidence for more than one thermal component in the X-ray spectrum of Geminga. In this Letter we present the results of an *Extreme Ultraviolet Explorer* (*EUVE*) observation of Geminga with the Deep Survey imager (DS), and a discussion of what can be learned from a joint analysis of this and several *ROSAT* observations.

2. OBSERVATIONAL DATA

Geminga was observed with *EUVE* for 9.3 days starting on 1994 January 14, during which an effective exposure time of 250,986 s was obtained in the DS. The time resolution was 8 ms. We extracted a total of 2472 counts from a circle of radius 43″. It is estimated that this aperture contains 2136 source photons and 336 background counts, while only 4% of the source photons fall outside it. Therefore, the true count rate is 0.0089 ± 0.0002 s^{-1}. Data were taken simultaneously by the three spectrometers pointed at the source, but no significant detection of the pulsar was made in these.

Three observations of Geminga were made with the *ROSAT* PSPC, in 1991 March, 1992 October, and 1993 September. Exposure times were 14,143, 4195, and 36,898 s, respectively. Total count rates were 0.525, 0.488, and 0.502 s^{-1}. The first observation was described by Halpern & Ruderman (1993) and the latter two by Halpern & Wang (1996). The *ROSAT* data were extracted from a circle of radius 150″, which is large enough to ensure that photons are not lost to the "ghost imaging" (Nousek & Lesser 1993; Snowden et al. 1994), which is significant below 0.2 keV.

3. SPECTRAL ANALYSIS

We confine our analysis to the blackbody plus power-law parameterization of the X-ray spectrum that was shown to be consistent with the *ROSAT* and *ASCA* data, namely,

$$F(E) = \left(C_1 \frac{E^3}{e^{E/kT} - 1} + C_2 E^{-\alpha} \right) e^{-\sigma(E) N_{\rm H}}$$

$$\text{keV cm}^{-2}\ \text{s}^{-1}\ \text{keV}^{-1}. \quad (1)$$

The alternative double blackbody model was ruled out (Halpern & Wang 1996). Figure 1 shows the confidence contours in the (T, $N_{\rm H}$) plane of such a fit to the 1991 *ROSAT* data, taken from Halpern & Ruderman (1993). Confidence limits are for three interesting parameters (T, $N_{\rm H}$, C_1). The fitted energy index α (not shown) is in the range 1.10–1.75 (68% confidence). The power-law component contributes less than 10% of the soft X-ray flux below 0.28 keV.

The Rayleigh-Jeans extrapolation of the fitted blackbody component corresponds to a predicted apparent visual magnitude *that is independent of the emitting area or the distance to*

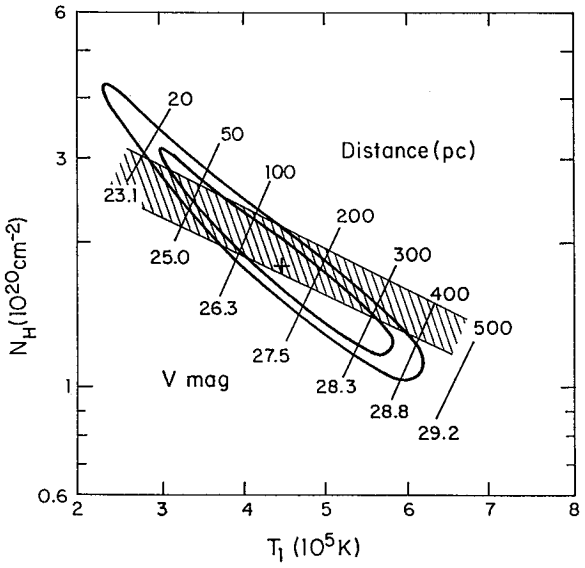

FIG. 1.—Confidence contours (68% and 90%) for the parameters of the blackbody component in the 1991 March *ROSAT* spectrum, for the case of three interesting parameters (T, N_H, C_1) (from Halpern & Ruderman 1993). Visual magnitudes are extrapolated from the Rayleigh-Jeans tail of the blackbody fit, while distances assume emission from the full surface of a 10 km radius star. The shaded region is that for which the observed count rate in the *EUVE* Deep Survey agrees to within ±20% of the value predicted by folding the corresponding *ROSAT* spectrum through the effective-area curve of the DS.

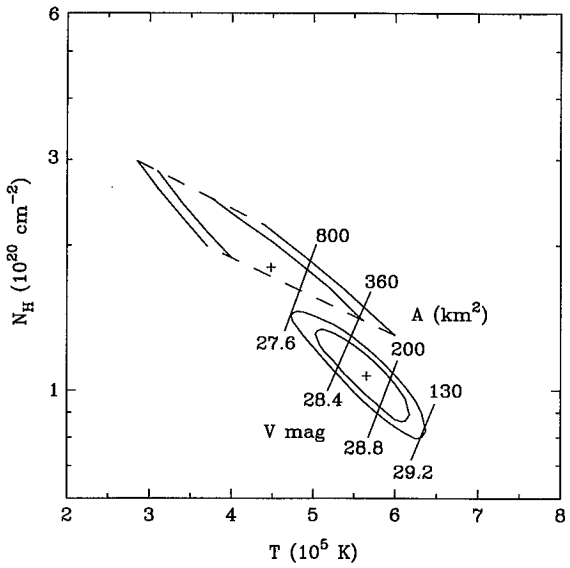

FIG. 2.—Lower confidence contours are for the 1993 September *ROSAT* observation, for the case of three interesting parameters (T, N_H, C_1). Visual magnitudes are extrapolated from the Rayleigh-Jeans tail of the blackbody fit, while areas are for an isotropically emitting sphere at a distance of 160 pc. Upper contours are the *EUVE/ROSAT* overlap region from Fig. 1.

the star, the latter because visual extinction is negligible. Contours of predicted visual magnitude for each of the acceptable blackbody fits are superposed on Figure 1. If we further assume that the emitting area is equal in size to a 10 km radius neutron star, then corresponding distances can be assigned to these contours. Adopting the parallax distance of 157^{+59}_{-34} pc from the *HST* (Caraveo et al. 1996), we see that the X-ray spectrum is consistent with a blackbody emitting neutron star at a temperature of (4–5) × 10^5 K. Since the corresponding predicted magnitudes are in the range 26.5–27.6, the visible flux from Geminga, with $V = 25.2 \pm 0.3$ (Halpern & Tytler 1988), cannot be the extrapolation of the blackbody but must be dominated by an additional contribution.

Although the DS is a broadband detector with no spectral resolution, we can evaluate the consistency of the DS count rate with the spectral models fitted to the *ROSAT* data. The details of this procedure were described by Halpern, Martin, & Marshall (1996) for the millisecond pulsar J0437−4715. In summary, each of the spectral models within the contours of Figure 1, with their individual fitted normalizations, are folded through the DS effective-area curve as given by Bowyer et al. (1996). A grid of predicted DS counts is thus derived for comparison with the observed number. The range of spectral parameters acceptable to the DS is approximated as those that predict a count rate within ±20% of the observed value of 0.0089 s^{-1}. The fact that the resulting band of spectral parameters, the shaded region in Figure 1, overlaps the *ROSAT* confidence contours, implies that the fluxes measured by the two instruments are in agreement. This result contradicts an analysis of the same data by Bignami et al. (1996), whose Figure 3 gives the impression that there is a factor of 10–100 discrepancy between the fluxes measured by *EUVE* and *ROSAT*.

Indeed, in the absence of variability it would be impossible for the fluxes measured by *ROSAT* and *EUVE* to differ by a large factor. Nearly all the flux from Geminga in the DS must fall in the wavelength range 65–110 Å because of the steep increase in interstellar absorption at longer wavelengths, even for a column density of only 1×10^{20} cm^{-2} (e.g., Fig. 5 of Halpern et al. 1996). Therefore, the DS flux comes mostly from the same soft thermal component that dominates in the overlapping *ROSAT* PSPC energy band. The resemblance of the DS pulse profile to that in the softest PSPC channels (see § 4) reinforces the conclusion that *EUVE* and *ROSAT* are seeing the same phenomena from Geminga, and that no additional components beyond one thermal and one nonthermal are necessary to explain all of the X-ray data.

We have repeated the same joint analysis with the 1992 and 1993 *ROSAT* observations. Although much briefer, the 1992 observation is also consistent with the DS count rate. However, the better statistics of the longer 1993 observation more narrowly restrict T and N_H to the ranges (5.0–6.2) × 10^5 K and (0.86–1.34) × 10^{20} cm^{-2}, respectively, at 68% confidence (lower contours of Fig. 2). The fitted energy spectral index α is $1.00^{+0.39}_{-0.27}$. Because of the hotter temperatures that fit the 1993 data, the surface area is restricted thereby to a range between 0.10 and 0.64 times the full area of a 10 km radius neutron star, while scaling as $(d/160\ \mathrm{pc})^2$. While this area is defined as that of an isotropically emitting sphere, areas that are significantly smaller than the full surface of the neutron star are also uncertain by a factor of a few because of projection effects that depend upon the unknown viewing geometry. Further modifications that arise in realistic atmospheres will be discussed in § 5.

For the 90% confidence range of spectral models shown in the lower contours of Figure 2, the predicted DS count rate falls between 0.0104 and 0.0168, with a best-fit value of 0.0136. Since the actual DS count rate is 0.0089 ± 0.0002, a mild disagreement between the *EUVE* and the 1993 *ROSAT* fluxes is indicated. However, if we take into account the ~20% systematic uncertainty in the effective area of the DS (Bowyer

et al. 1996), then the discrepancy is barely significant. Moreover, there were systematic changes of comparable magnitude in the behavior of the PSPC later in the mission. One is a second-order decrease in the gain (Prieto, Hasinger, & Snowden 1996). Another is a possible increase in the transmission of the detector entrance window, which is only partly taken into account in the new response matrix (Hasinger & Snowden 1994). Both of these effects act in the right direction to explain the discrepancy by increasing the *ROSAT* counts in the softest energy channels. Added to these instrumental effects could be variability of Geminga itself by a few percent (see § 4). Therefore, any attempt to find a more exotic cause for the small discrepancy noted here would not be well motivated.

4. TIMING ANALYSIS

The most accurate ephemeris for the spin parameters of Geminga comes from ongoing EGRET observations. We use the ephemeris of Mattox, Halpern, & Caraveo (1996), which is based on the first 4 years of EGRET data, for the analysis of all other data. This ephemeris is accurate to within 0.02 revolutions for the years 1991–1995. There has been no detectable timing noise during this period. We take into account the proper motion of the pulsar (Bignami, Caraveo, & Mereghetti 1993; Mignani, Caraveo, & Bignami 1994; Caraveo et al. 1996), although its effects on the broad X-ray pulse profiles are not significant over such a short time span. The stability of the spacecraft clocks and the accuracy of their conversion to ephemeris time have been discussed elsewhere in reference to Geminga (Halpern & Wang 1996) and to the 5.75 ms pulsar PSR J0437−4715 (Halpern et al. 1996). We conclude that the *EUVE* timing is accurate to within the 8 ms time resolution of these data, and that the *ROSAT* timing is about a factor of 2 better.

Figure 3 shows the soft X-ray pulse profiles of all the *EUVE* and *ROSAT* data in absolute phase. We restrict the *ROSAT* data to the energy range 0.08–0.28 keV, which largely overlaps the band detected by *EUVE*. Background has been subtracted from the *EUVE* data (it is insignificant for *ROSAT*), and the ordinates have been scaled in proportion to the exposure times of the *ROSAT* observations in order to facilitate comparison of their pulse profiles. Measured pulsed fractions are given in each panel. It is immediately apparent that the pulse profile changed with time. In the original 1991 observation, the pulse had considerable high-frequency structure, and the pulsed fraction was 0.32 ± 0.05. By 1993 the pulsed fraction had declined to 0.18 ± 0.02, and most of the fine structure had disappeared. The 1994 *EUVE* data, although noisier, has a pulsed fraction of 0.18 ± 0.06, the same as the most recent *ROSAT* observation. In addition, there is a marginally significant second peak in the *EUVE* light curve that may be similar to structure in the two earlier *ROSAT* observations.

A more complete discussion of the *ROSAT* data across the full PSPC energy band is presented by Halpern & Wang (1996). We considered whether or not instrumental effects could be responsible for the observed variations, and concluded that they were not. The behavior of the higher energy PSPC data is important in ruling out smearing due to timing errors, because the pulsed fraction of the harder X-rays did not decrease with time, and may even have increased. The known drift in detector gain is probably not responsible, because the pulse shape is a relatively broadband phenomenon, and the gain shift is much smaller than the resolution of the detector. Finally, confirmation of the *lowest* observed pulsed fraction by a different instrument, the *EUVE* DS, convinces us of the reality of the effect.

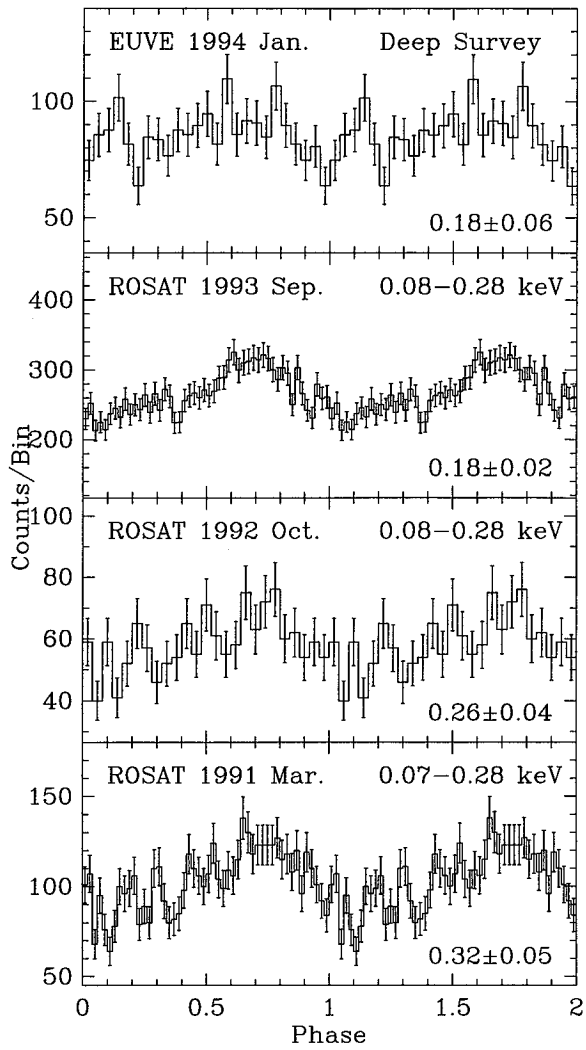

FIG. 3.—Comparison of the soft X-ray light curves of Geminga from *EUVE* and *ROSAT*. Pulsed fractions are indicated at the lower right of each panel. Phase 0 corresponds to MJD 48,749.999999259 (TDB) according to the ephemeris of Mattox, Halpern, & Caraveo (1996).

The fine structure in the 1991 data is best described as dips, superposed on a light curve that otherwise remained quite similar in 1993. It is the dips that are largely responsible for the change in pulsed fraction, as the pulsed X-rays are defined as those which lie above the minimum in the light curve. Finding it difficult to understand narrow dips in terms of rotational modulation of thermally emitting regions on the surface, Halpern & Ruderman (1993) attributed this effect to cyclotron resonant scattering in a plasma-filled magnetosphere on the closed field lines. The required high density of $e^{\pm}$ pairs was assumed to accumulate there from the conversion of primary high-energy γ-rays and secondary radiation on the strong B field near the surface. It is tempting to speculate that the decrease of such structure in the light curve is evidence for the disappearance of the scatterers, namely, an emptying of the closed magnetic field lines of $e^{\pm}$ pairs. Perhaps the small changes observed in the higher energy X-rays (Halpern &

Wang 1996) are associated with processes that resupply plasma to the magnetosphere at a variable rate.

5. MODEL ATMOSPHERES AND OPTICAL EMISSION

Of course a blackbody analysis is too naive, because the effects of magnetized neutron star atmospheres can be considerable at the temperatures considered here. Although we do not fit such models here, the likely results of such an analysis can be anticipated from previous work on the first *ROSAT* data by Meyer, Pavlov, & Mészáros (1994). Using a magnetized hydrogen atmosphere model, they concluded that the effective temperature $T_{\rm eff}$ is 2–3 times smaller than the fitted blackbody value. In their model, the observed spectral hardness is an effect of decreasing opacity at higher energies, for which the radiation emerges from deeper in the atmosphere. Although Meyer et al. (1994) did not use the response matrix appropriate to the earlier *ROSAT* data, the general trend of their results is almost certainly correct.

Accompanying the lower effective temperature was a decrease in distance required by the model, to a value that was highly uncertain but could be as low as 40 pc or as high as 140 pc. These distance estimates were for a 10 km radius neutron star. Since a distance less than 120 pc is ruled out by the small observed parallax, the room for consistency between the model atmospheres and the observations is much reduced. Rather than straining against the limits of the measured distance, the atmosphere models can now instead be usefully interpreted in terms of the size of the emitting region. In particular, larger emitting areas are implied which may cover the majority of the stellar surface, instead of the 0.10–0.64 fraction mentioned above.

Atmosphere models are not the cause or cure of any major disagreement between the *EUVE* and *ROSAT* data as proposed by Bignami et al. (1996), since we have shown that discrepancy to be fictitious. Atmosphere models simply reproduce the same X-ray flux at lower effective temperature. For the same reasons that adequate blackbody fits to the *EUVE* and *ROSAT* data delineate almost the same strip in parameter space in Figure 1, an atmosphere model that fits the *ROSAT* data will also fit the *EUVE* flux in the same energy band.

Similarly, atmospheres do not increase the contribution of surface thermal emission to the optical emission (for a given distance), since the low-energy flux closely follows a Rayleigh-Jeans law corresponding to a temperature slightly *lower* than $T_{\rm eff}$ (Meyer et al. 1994). Even if the thermal X-ray emission comes from only part of the neutron star, the rest of the surface is too cool to supply the majority of the visible flux. The opposite conclusion was mistakenly drawn by Bignami et al. (1996), who claimed that the optical emission from Geminga is consistent with thermal emission from a neutron star of radius 10–15 km at a temperature of only $(2.2–2.8) \times 10^5$ K. This is because there is an error in their blackbody formula; the curves in their Figures 3 and 4 are too high by a factor of $\simeq 3$. In contrast to the observed $V = 25.2$, the cool blackbodies hypothesized by Bignami et al. (1996) would have $V = 26.8–28.0$ at a distance of 160 pc, and a real neutron star would be even fainter if its $T_{\rm eff}$ had those same values. But they do correctly show that the optical colors are inconsistent with a Rayleigh-Jeans spectrum, as did Bignami, Caraveo, & Paul (1988). We agree, as did Halpern (1989), that there is a real peak in the V-band, and that it requires the visible flux to be dominated by some nonthermal mechanism, possibly the ion-cyclotron feature suggested by Bignami et al. (1988). The observed B magnitude of 26.5 ± 0.5 is closer to the blackbody extrapolation, and could have a significant thermal contribution.

Finally, we note that while the extrapolation of the blackbody falls below the optical, the fitted power-law component would greatly exceed it. The power-law index $\alpha = 1.00^{+0.39}_{-0.27}$ extrapolates to visual magnitudes of 18.2–22.4. While the power-law model is only a parameterization, which may not be valid even in the X-ray range, it does serve to remind us that any hypothesized nonthermal power law extending from the optical to the X-ray must have an energy spectral index α_{ox} less than 0.3, considerably flatter than the energy index in the X-ray band itself. A future test of whether the thermal or nonthermal component is responsible for the optical flux could be made by observing optical and UV pulsations, and comparing them to the soft and hard X-ray light curves.

This work was supported by NASA grants NAG 5-2569, NAG 5-1935, and NAG W-4482. This paper is Contribution 611 of the Columbia Astrophysics Laboratory.

REFERENCES

Bertsch, D. L., et al. 1992, Nature, 357, 306
Bignami, G. F., Caraveo, P. A., & Mereghetti, S. 1993, Nature, 361, 704
Bignami, G. F., Caraveo, P. A., Mignani, R., Edelstein, J., & Bowyer, S. 1996, ApJ, 456, L111
Bignami, G. F., Caraveo, P. A., & Paul, J. A. 1988, A&A, 202, L1
Bowyer, S., Lampton, M., Lewis, J., Wu, X., Jelinsky, P., & Malina, R. F. 1996, ApJS, 102, 129
Caraveo, P. A., Bignami, G. F., Mignani, R., & Taff, L. G. 1996, ApJ, 461, L91
Halpern, J. P. 1989, in Proc. *GRO* Science Workshop, ed. W. N. Johnson (Greenbelt: GSFC), 4-166
Halpern, J. P., & Holt, S. S. 1992, Nature, 357, 222
Halpern, J. P., Martin, C., & Marshall, H. L. 1996, ApJ, 462, 908
Halpern, J. P., & Ruderman, M. 1993, ApJ, 415, 286
Halpern, J. P., & Tytler, D. 1988, ApJ, 330, 201
Halpern, J. P., & Wang, F. Y.-H. 1997, ApJ, in press
Hasinger, G., & Snowden, S. 1994, in The *ROSAT* Users' Handbook, ed. U. G. Briel et al. (Garching: MPI), 47
Mattox, J. R., Halpern, J. P., & Caraveo, P. A. 1996, A&A, in press
Meyer, R. D., Pavlov, G. G., & Mészáros, P. 1994, ApJ, 433, 265
Mignani, R., Caraveo, P. A., & Bignami, G. F. 1994, Messenger, 76, 32
Nousek, J. A., & Lesser, A. 1993, US *ROSAT* Sci. Data Center Newsletter, No. 8, 13
Prieto, M. A., Hasinger, G., & Snowden, S. L. 1996, A&A, in press
Snowden, S. L., McCammon, D., Burrows, D. N., & Mendenhall, J. A. 1994, ApJ, 424, 714